Kinetics of CO_2 capture with calcium oxide during Direct Air Capture in a fluidised bed

Bryan Kean Hong Ooi[1], Ewa J. Marek[1*]

[1] Department of Chemical Engineering and Biotechnology, University of Cambridge, Philippa Fawcett Drive, CB3 0AS, United Kingdom

[*]Corresponding author(s): ejm94@cam.ac.uk

Abstract

The bulk of research in carbon capture involves high CO_2 concentrations. This work instead describes the kinetics of CaO carbonation in mixtures with pCO_2 between 0.38 to 2.70 vol% and at temperatures between 400 and 650°C. The reaction was studied in a bed of SiO_2 fluidised at flowrates corresponding to U/U_{mf} of ~4. Lower concentrations of CO_2 connected to the rates of mass transfer of CO_2 of the same order of magnitude as the rates of carbonation, thus, were eliminated from the kinetic analysis. The introduction of steam to the gas mixture (2 vol%) increased the rates of carbonation, demonstrating a pseudo-catalytic effect, yet diminishing at higher temperatures. A rate expression generally accepted in literature for high concentration CO_2 in CaO carbonation was assessed for its applicability at near-equilibrium conditions, demonstrating that the order of the rate expression changes between 0 and 1, increasing at higher temperatures. Using non-linear regression, the experimental values were fitted to the Langmuir-Hinshelwood rate expression. The obtained parameters indicate CO_2 sorption and desorption being equilibrated, with the overall capture dominated mainly by slow kinetics of chemical reactions.

Keywords: Direct Air Capture, DAC, CaO, fluidised bed, kinetics

1. Introduction

The effects of anthropogenic CO_2 on climate change are increasingly worrisome. With global temperatures setting record highs annually, the need for cost-effective solutions to actively remove CO_2 from the atmosphere is ever more pressing.

Multiple solid sorbents have been proposed as potential candidates for CO_2 capture, including CaO, MgO, alkali-metal oxides, and their modified versions designed to overcome certain material-related problems such as sintering [1–4]. In general, these oxides react with CO_2 to form carbonates in a reversible reaction. The alkali-based sorbents have been extensively studied for CO_2 capture in high CO_2 concentrations, simulating flue gas conditions from power plants, steel industry and cement production (up to 40,000 ppm CO_2). While necessary to design

point-source carbon capture solutions, these studies omit lower CO_2 concentrations, including the two orders of magnitude lower levels of CO_2 in air (~420 ppm CO_2) [5–8]. Addressing such a gap is needed to assess the potential of solid sorbents in Direct Air Capture (DAC), where CO_2 is separated from ambient air.

The interest in CaO for DAC stems from its relatively high theoretical gravimetric uptake of 0.786 $\mathrm{g_{CO_2}\,g_{sorbent}^{-1}}$ compared to other potential solid sorbents such as BaO with 0.288 $\mathrm{g_{CO_2}\,g_{sorbent}^{-1}}$ [9]. However, the capacity of CO_2 uptake with CaO is often lower than the stoichiometrically expected uptake, maintaining only ~0.15 $\mathrm{g_{CO_2}\,g_{sorbent}^{-1}}$ after hundreds of carbonation-decarbonisation cycles and the unavoidable material deactivation. The challenge of low CO_2 uptake capacities will likely be encountered in realistic DAC applications [10] but CaO remains a good candidate because of its application in the cement industry which can utilise the spent sorbent.

Calcium oxide undergoes a reversible carbonation-calcination process, $CaO+CO_2 \rightleftharpoons CaCO_3$, also underpinning the technology called calcium looping. In the reversible loop, the forward or backward reactions dominate according to the thermodynamic constraints described by the equilibrium partial pressure of CO_2, $p_{CO_2,eq}$, at a given temperature T. For CaO, the $p_{CO_2,eq}$ quickly approaches $p_{CO_2,air}$ which limits the CaO's application for direct air capture to only low temperatures. The equilibrium $p_{CO_2,eq}$ as a function of temperature can be calculated taking from thermochemical data sets, *e.g.* [11]:

$$p_{CO_2,eq} = \exp\left(\frac{-20809}{\mathrm{T_{eq}}} + 18.427\right) \quad (1)$$

where $p_{CO_2,eq}$ is in atm and T_{eq} is in K. The equilibrium curve of the CaO-$CaCO_3$ system is illustrated in Fig. 1. At 40,000 ppm CO_2 and atmospheric pressure, carbonation of CaO is thermodynamically favourable up to approximately 690°C, compared to only 520°C for 420 ppm CO_2 in air.

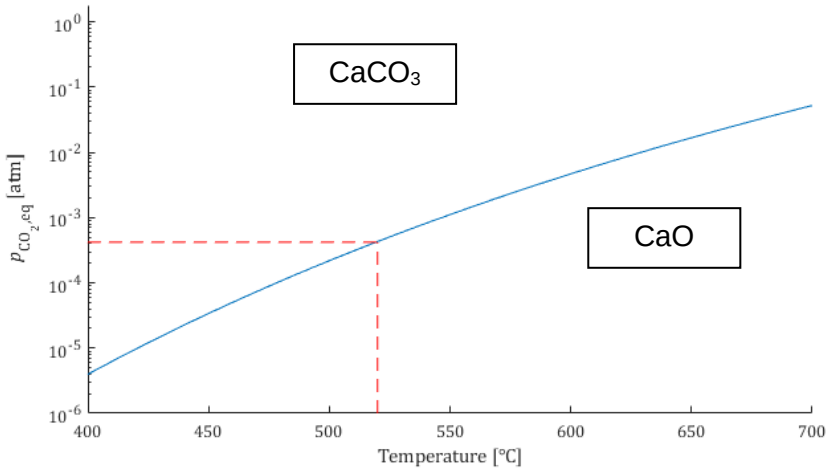

Fig. 1: Equilibrium partial pressure of CO_2, $p_{CO_2,eq}$ plotted against temperature. FactSage thermodynamics database was used to compute the $p_{CO_2,eq}$ [13]. Red dashed line indicates $p_{CO_2,eq} \approx 420 \times 10^{-6}$ atm, *i.e.* CO_2 concentration in air.

Most of the earlier works proposed that the surface reaction of CaO carbonation involves a two-step mechanism with the adsorption of CO_2 onto the surface followed by the chemical reaction to form $CaCO_3$ [1,12,13], *viz.*

$$\mathrm{CaO} + \mathrm{L} + \mathrm{CO_2} \rightleftharpoons \mathrm{CaO} + \mathrm{L(CO_2)}$$
$$\mathrm{CaO} + \mathrm{L(CO_2)} \rightleftharpoons \mathrm{CaCO_3} + \mathrm{L}$$

where L refers to an active site of CaO, and $\mathrm{L(CO_2)}$ to the site occupied by CO_2. Experimentally, the rate of carbonation, r was then described by the power law as:

$$r = k_A\left(p_{CO_2} - p_{CO_2,eq}\right)^n \tag{2}$$

where k_A is the rate constant and n is the order of reaction.

Sun *et al.* proposed that the $CaCO_3$ formation and decomposition step is often equilibrated at low pCO_2 values; thus, the adsorption step is rate-controlling [12]. They found that $n = 1$ for cases with low driving force, *i.e.* when $\left(p_{CO_2} - p_{CO_2,eq}\right)$ <10 kPa, turning into n =0 when the pressure difference exceeds ~10 kPa, which the authors associated with the chemical reaction becoming rate-controlling [12]. Multiple other authors confirmed $n = 1$ in eq. (2); *e.g.* Yu and Fan gave $n = 1$ for $\left(p_{CO_2} - p_{CO_2,eq}\right) < 80$ kPa at 700°C [13], while Scaltsoyiannes *et al.* extended this result for $\left(p_{CO_2} - p_{CO_2,eq}\right) < 117$ kPa between 670 and 820°C [1]. Similar studies are lacking for CaO reacting with CO_2 at temperatures and concentrations relating to direct air capture. The broad range of the existing work suggests that for low driving force expected in DAC, *i.e.* $p_{CO_2} \sim p_{CO_2,eq}$, we should expect $n = 1$.

Our work focuses on the CaO carbonation at low CO_2 concentrations, similar to those in Direct Air Capture, to verify whether the expected rate expression remains a simple power-law with $n = 1$ at the unavoidably low driving forces. Additionally, we investigate the competing interplay between the driving force (concentration difference) for CO_2 uptake, which is maximised for DAC with CaO at low temperatures, and the kinetic constant, k, which is low at low temperatures. Because both the driving force and the kinetic constant are strongly dependent on temperature, we performed the experimental work in a fluidised bed to ensure quick heat distribution. Similarly, because of the limited driving force for reaction, we assessed the potential limitations from CO_2 delivery to ensure that the obtained rates of reactions remain in the kinetically controlled regime. This comprehensive approach adds to the discussion on CaO potential in direct air capture.

2. Experimental

Silica sand was used as a bed material. A batch of Fraction D sand obtained from David Ball Specialist Sands was washed and sieved to 200–250 μm. Similar size particles, 150-200 μm, of quicklime were obtained by grinding and sieving the Calbux commercial product from Lafarge Tarmac. The XRD analysis provided information about the composition of in quicklime particles: 96 wt.% CaO, 4 wt.% $CaCO_3$ and negligible amounts of $Ca(OH)_2$. The X-ray diffraction (XRD) profile for the quicklime used in this work is shown in Fig. S1 in the Supplementary Information (SI).

A schematic of the experimental setup is illustrated in Fig. 2. Gases, N_2 and CO_2, were taken from the laboratory supply of reticulated gases with flowrates controlled with a rotameter and mass flow controller (Alicat MC-200SCCM), respectively. The flows were then connected and the resulting CO_2-N_2 mixture fed into an electrically heated quartz reactor (i.d. 30 mm). The achieved concentrations of CO_2 spanned from 0.38 to 2.70 vol%. The quartz tube contained a porous alumina disk, positioned ~17 cm from the gas inlet. The disk held the solid particles of SiO_2, used as the main bed material. A type K thermocouple measured the temperature ~1 cm above the distributor, with readings used to control the temperature setpoint in experiments. The top of the reactor was covered with a loosely fitted plate to minimise air ingress. A sampling line was inserted from the top, with the sampling flow induced by a vacuum pump. The sample gas passed through a particulate filter, then a CO_2 sensor (Gas Sensing Solutions SprintIR WHF-5) before being vented to the local exhaust.

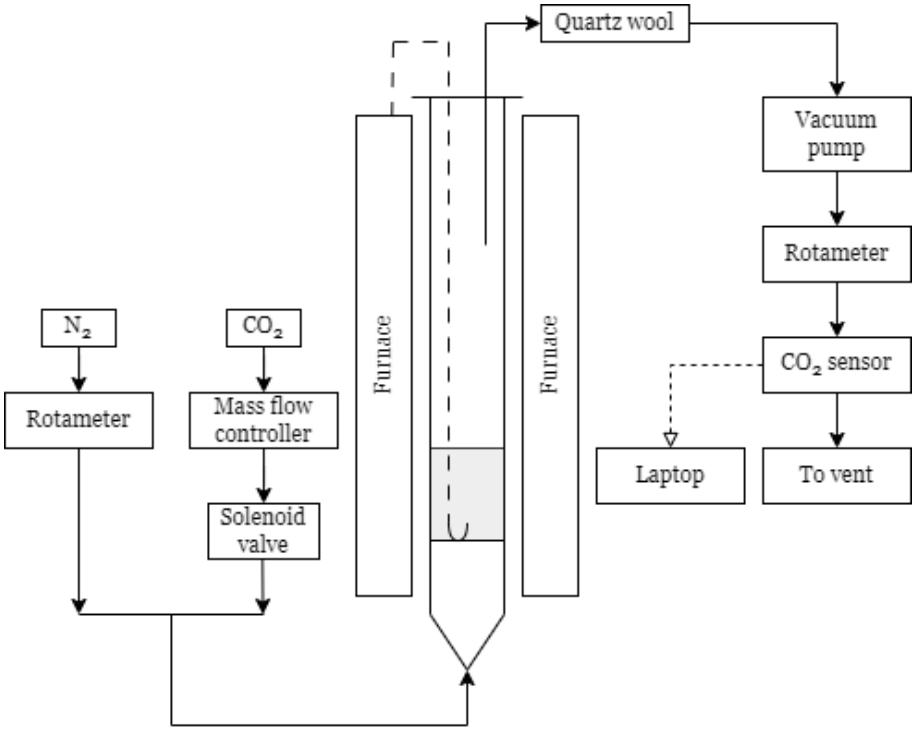

Fig. 2: Schematics of the fluidised bed rig. Not illustrated are the desiccant and bubbler for wet carbonation. The desiccant was placed between the vacuum pump and quartz wool, while the bubbler was placed downstream of the mixing of N_2 and CO_2, and upstream of the inlet to the fluidised bed.

Carbonation of CaO in the presence of steam was performed by bubbling the CO_2-N_2 gas mixture through a bubbler filled with water at 20°C upstream of the inlet fluidised bed reactor. Calcium chloride ($CaCl_2$) desiccant was then used to remove steam from the sampled gas stream before directing it to the CO_2 sensor.

Experiments with 30 g of silica sand (200 – 250 μm) as the bed material were carried out at temperatures between 400 and 650°C, with 50°C increments. The gas flowrates were adjusted with temperature, keeping the ratio of U/U_{mf} ~4. Samples of quicklime (~20 mg, 150-200 μm) were introduced into the reactor from the top.

The reaction between CO_2 in the incoming gas and CaO was monitored by recording the CO_2 depletion in the sampled gas. Each experiment was carried out three times. Exemplary results are presented in Fig. 3. Initially, a constant concentration over time was observed, decreasing upon the introduction of the sample, when the CaO reacted with CO_2. When the reaction finished, the CO_2 concentration returned to the original value. The measured CO_2 profiles were processed to account for mixing in the freeboard in the analyser – the deconvolution procedure is described in the SI, Section 2.

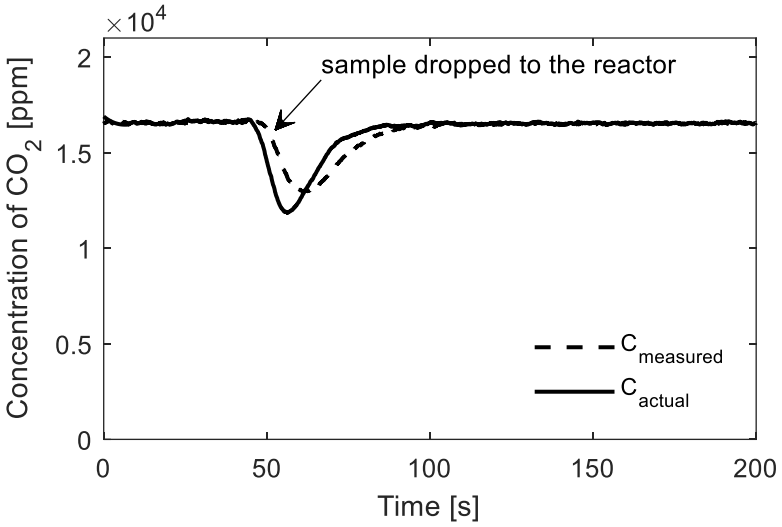

Fig. 3: Example plot of CO_2 concentration over time after introducing a batch of CaO sample. The lines present the measured concentration ($C_{measured}$) and the deconvoluted result when accounting for mixing times in the sampling line (C_{actual}).

During the experiments, the total molar flowrate through the reactor varied because of the CO_2 uptake. In the experiments with steam, the flowrate that passed through the CO_2 analyser was dried, so the CO_2 fraction was different to that in the reactor. To account for these differences, flowrates at the outlet were calculated by performing mass balances, as described in the SI, Section 2. The obtained consumption of CO_2 over time, $F_{CO_2,2}(t)$ in mol/s was normalised by the mass of CaO introduced, m_{CaO}, arriving at the rate expression as: $r(t) = \frac{F_{CO_2,2}(t)}{m_{CaO}}$. For assessing the kinetic parameters of carbonation, the maximum rates of reaction, r_{max} were taken, assuming the conversion of the CaO particle was, at that stage, negligible.

Thus, our analysis does not provide information on the rate dependency *vs* the CaO conversion. Such dependency, $f(X)$, would describe how a particle of CaO reacts in the presence of the product $CaCO_3$ and upon the whole duration of the process. Instead, here, we only focus on the starting moments for CaO carbonation. To check that all our data points indeed correspond to low X, we plotted the collected rates *vs* conversion in Fig. S6 in the SI, confirming that all samples were analysed at very low conversions, so our assumption of $X \sim 0$ is justified.

To present how the conversion of CaO particles changes upon experiments, we plotted X vs time in Fig. S7 of the SI. Because the collected signal for CO_2 uptake was low, most of the observed CaO conversion corresponded to relatively large experimental errors. Taking r_{max} for assessing kinetics helps minimise the impact of these errors.

The conversion of CO_2 introduced to the reactor was <20%, thus, for simplicity we assume a differential reactor. For a given temperature, a minimum of three sets of experiments were performed, varying the driving force ($p_{CO2} - p_{CO2,e}$). Each experiment was carried out three times.

3. Theory

The overall uptake and release of CO_2 on calcium oxide can be written as

$$\mathrm{CaO} + \mathrm{CO_2} \rightleftharpoons \mathrm{CaCO_3} \tag{4}$$

Most studies of CaO carbonation agree that the process employs a Langmuir-Hinshelwood mechanism [14,15] involving a surface adsorption-desorption step (R1) and a chemical reaction step (R2) *viz.*

$$\mathrm{CaO} + \mathrm{L} + \mathrm{CO_2} \underset{k_D}{\overset{k_A}{\rightleftharpoons}} \mathrm{CaO} + \mathrm{L(CO_2)} \tag{R1}$$

$$\mathrm{CaO} + \mathrm{L(CO_2)} \underset{k_2}{\overset{k_1}{\rightleftharpoons}} \mathrm{CaCO_3} + \mathrm{L} \tag{R2}$$

where L refers to unoccupied active sites, and $\mathrm{L(CO_2)}$ refers to active sites occupied by adsorbed CO_2.

Rates of the elementary steps in R1 and R2 are:

$$r_A = k_A(1-\theta)p_{CO_2} \tag{5}$$

$$r_D = k_D\theta \tag{6}$$

$$r_1 = k_1\theta \tag{7}$$

$$r_2 = k_2(1-\theta) \tag{8}$$

where θ is the fraction of active sites occupied by CO_2, and k_A, k_D, k_1 and k_2 refer to the rate constants of the adsorption, desorption, carbonation, and calcination steps, respectively.

In some works, R2 is replaced by a version presented as R3 [12], where the creation of $CaCO_3$ consumes the active site on the CaO surface, so the pool of L varies with particle conversion:

$$\mathrm{CaO} + \mathrm{L(CO_2)} \underset{k_2}{\overset{k_1}{\rightleftharpoons}} \mathrm{CaCO_3} \tag{R3}$$

Then, consequently, $r_2 = k_2$. Both mechanisms are often collapsed into a simplified rate expression, $r = k_A\left(p_{CO_2} - p_{CO_2,eq}\right)^n$, where n, the order of reaction, varies from 0 to 1 and depends on the rate-limiting steps.

Sun *et al.* proposed that at low p_{CO_2}, the chemical reaction step was rapid compared to the surface adsorption-desorption step [15]. This meant that adsorbed CO_2 molecules were

rapidly consumed in the carbonation reaction to produce $CaCO_3$, *i.e.* $\theta \ll 1$. Therefore, the surface adsorption-desorption step was rate controlling, *i.e.* $r = r_A - r_D$

$$r = k_A(1-\theta)p_{CO_2} - k_D\theta \quad (9)$$

Substituting for θ and rearranging eq. (9) yielded

$$r = k_A\left(p_{CO_2} - p_{CO_2,eq}\right) \quad (10)$$

For the case where $\left(p_{CO_2} - p_{CO_2,eq}\right)$ had a zero-order relation with r, Sun *et al*. postulated that at a critical value of $\left(p_{CO_2} - p_{CO_2,eq}\right) \approx 10$ kPa, the fraction of active sites with adsorbed CO_2, θ could no longer be assumed as low. In fact, they surmised that the driving force of CO_2 for adsorption was high enough such that the active sites became mostly saturated, *i.e.* $\theta \approx 1$. At this stage, the chemical reaction step was rate-limiting. Thus, $r = r_1 - r_2$ *viz.*

$$r = k_1\theta - k_2(1-\theta) \quad (11)$$

$$r = k_1 \quad (12)$$

This means that the rate switches from the first order into a zero-order, depending on the driving force.

Interestingly, a different dominating mechanism was assumed by Ortiz *et al.* [15] The authors state that gas-solid reactions are commonly limited by the chemical reaction step being slower than the adsorption step. Still, they arrive at the rate expression of the form similar to eq. (10), where the driving force $\left(p_{CO_2} - p_{CO_2,eq}\right)$ had a first-order relation with r but the kinetic constant related to the chemical reaction step, k_1.

For a small driving force $\left(p_{CO_2} - p_{CO_2,eq}\right)$, the process can quickly become limited by mass transfer rather than adsorption or chemical reactions. In a fluidised bed, the reacting solid CaO particles are distributed in the particulate, emulsion phase, while the gas with CO_2 is divided between the bubble and particulate phases. An efficient exchange of gas between the two phases is needed, otherwise the reaction in the emulsion phase will lead to the local depletion of CO_2, and the process might become limited by interphase mass transfer. The interchange of gas between bubbles and the particulate phase can be described by the crossflow factor, X, which describes the number of times the bubble volume is exchanged while a bubble moves through the bed. Here, the crossflow factor was assessed using the correlation developed by Davidson and Harrison [16] using the potential flow theory.

$$X = \frac{6.34H_{mf}}{d_B(gd_B)^{0.5}}\left[U_{mf} + \frac{1.3\varepsilon_{mf}D_{CO_2}^{0.5}g^{0.25}}{\left(1+\varepsilon_{mf}\right)d_B^{0.25}}\right] \quad (13)$$

where d_B is the diameter of a bubble, H_{mf} is the height of the bed at the minimum fluidisation conditions, ε_{mf} is the bed voidage at minimum fluidisation taken as 0.46. The solution for X

requires finding the bed height, H, the mean diameter of bubbles, d_B and the velocity of bubbles, U_B, simultaneously [17]. The applied correlations are listed in the SI, Section 3.

For the described experiments, the crossflow factor was between 1.6 at 600°C to 3.5 at 400°C. The study by Hernández-Jiménez *et al.* [18] assessed that the correlation for X based on the potential flow theory underestimates the values of X. Overall, the values of X here suggests a good mixing of gas between the two phases.

When the CaO particle is introduced to the emulsion phase, the CO_2 for reaction needs to transfer through a boundary layer around the sorbent particle to its surface. Assuming a pseudo-steady-state, the minimum rate of mass transfer through this boundary film can be calculated using Fick's law for a dilute binary mixture of CO_2 and N_2 (expressed as species A and B, respectively),

$$N_A = -4\pi r^2 D_{AB} \frac{dC_A}{dr} \tag{14}$$

where r represents the radial coordinate, D_{AB} is the binary diffusion coefficient between A and B, and $\frac{dC_A}{dr}$ represents the concentration gradient of A in spherical coordinates. Equation (13) can be integrated with the boundary conditions at the particle surface (r_p) and at the coordinate representing the distance from the particle surface to the end of the gas film (δ):

$$\text{at r} = r_p\ , \quad C_A = C_{A,s}$$
$$\text{at r} = \delta\ , \quad C_A = C_{A,b}$$

where $C_{A,s}$ is the minimum concentration of CO_2 on the surface of the particle taken as $\frac{p_{CO_2,eq}}{RT}$ at T, $C_{A,b}$ is the bulk concentration of CO_2 taken as $\frac{p_{CO_2}}{RT}$ at T.

$$N_A = 4\pi D_{AB} \left(\frac{C_{A,s} - C_{A,b}}{1/\delta - 1/r_p} \right) \tag{15}$$

Normalising N_A by the mass per particle of CaO,

$$n_A = \frac{3N_A}{4\pi r_p^3 \rho_p} = 4\pi D_{AB} \left(\frac{C_{A,s} - C_{A,b}}{1/\delta - 1/r_p} \right) \frac{3}{4\pi r_p^3 \rho_p} \tag{16}$$

where ρ_p is the mass density of CaO. The resulting units for n_A is $\mathrm{mol\,s^{-1}\,g_{CaO}^{-1}}$. The thickness of the film layer was calculated after Hayhurst [36] as $\mathrm{Sh} = 2\varepsilon_{mf}\left(1 + \frac{r_p}{\delta}\right)$, where ε_{mf} is the bed voidage at minimum fluidisation taken as 0.46, and Sh is the Sherwood number, calculated as $\mathrm{Sh} = 2\varepsilon_{mf} + 0.7\left(\frac{\mathrm{Re}_{mf}}{\varepsilon_{mf}}\right)^{\frac{1}{2}} \mathrm{Sc}^{\frac{1}{3}}$.

4. Results and discussion

Before assessing the kinetic parameters, we screened the obtained results, eliminating the data points where the rate of CO_2 delivery was less than an order of magnitude faster than the rate of carbonation, *i.e.* $n_A/r_{max} < 10$. This eliminated a range of experiments at 500℃ and 600℃ when applying p_{CO_2} near ambient CO_2 concentrations (~420 ppm). This is because at higher temperatures the values of Re_{mf} are lower, leading to a lower flow rate of gas to reach the desired U/U_{mf}. Moreover, for higher temperatures the rate of reaction, r_{max} increases exponentially with temperature. If DAC were to be performed in a bubbling fluidised bed above 400°C, the process would likely be limited by external mass transfer.

Taking the rate expression as $r = \mathrm{k_A}\left(p_{CO_2} - p_{CO_2,eq}\right)$, *i.e.* eq. (2) with $n = 1$, we can plot The values of k_A can be extracted by rearrangement

$$k_A = \frac{r}{\left(p_{CO_2} - p_{CO_2,eq}\right)} = A\exp\left(-\frac{E_a}{RT}\right) \tag{17}$$

where E_a is the activation energy, A is the pre-exponential factor, R is the ideal gas constant, and T is temperature. Then, the constants A and E_a can be computed from the Arrhenius plot, $\ln(k_A) = -\frac{E_a}{RT} + \ln(A)$, presented in Fig. 4.

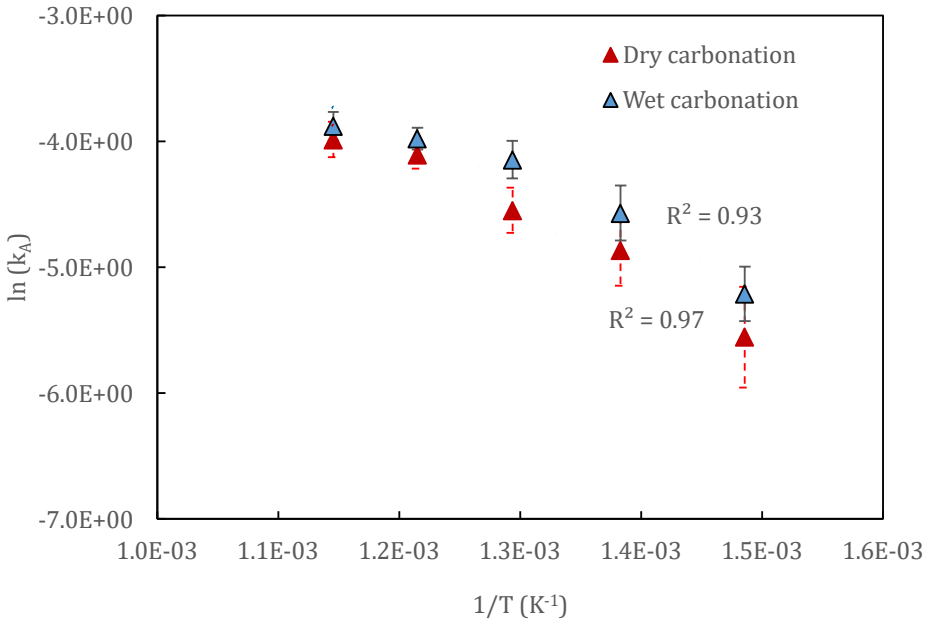

	E_a [kJ mol^{-1}]	A [mol s^{-1} g$_{\mathrm{CaO}}^{-1}$ atm^{-1}]
Wet carbonation	39.0 ± 3.9	4.56 ± 2.11
Dry carbonation	33.8 ± 3.6	2.58 ± 1.13

Fig. 4: Plot of $\ln(k_A)$ against $1/T$ where k_A was extracted by using eqn. (17), $i.e.$ taking $n = 1$. The error bars indicate the 95% confidence intervals for each temperature data set (9 experiments).

From the intercepts and slopes, we obtained E_a, which are higher than those reported previously in studies with high concentrations of CO_2, when assuming $n = 1$, *e.g.* 22-29 kJ/mol in [1,12]. On the other hand, Sun *et al.* predicted E_a of 41.5 kJ/mol, so close to the values in Fig. 4, from the kinetic parameters of $CaCO_3$ calcination reaction and the equilibrium constant. They ascribed the discrepancy to their experimentally obtained kinetics to the fact that equilibrium is likely not affecting the start of carbonation.[12]

From Fig. 4, wet carbonation resulted in higher rates, and so k_A for across all temperatures investigated, with Fig. 5 also demonstrating higher rates for all $(p_{CO_2} - p_{CO_2,eq})$, as compared to dry carbonation, *i.e.* the pseudo-catalytic effect. Manovic and Anthony reported that while steam enhanced the rate of carbonation, the effect was more pronounced at lower temperatures [19]. However, this enhancement on the rate of carbonation was only observed in the diffusion-limited regime, *i.e.* the conversion of CaO to $CaCO_3$ after r_{max}. They attributed the enhanced rate of carbonation to the ability for steam to improve solid state diffusion through the $CaCO_3$ product layer. The results in Figs. 4 and 5 show the catalytic effects also in the kinetically-controlled regime. However, the error bars depicting the 95% confidence intervals for dry and wet carbonation overlap for 400℃ and 450℃. This indicates that the benefits of steam at 400 ℃ and 450 ℃ are not significantly pronounced. Moreover, the difference between r_{max} for wet and dry carbonation decreases with increasing temperature, further indicating diminishing returns from the addition of steam on r_{max} with increasing temperatures.

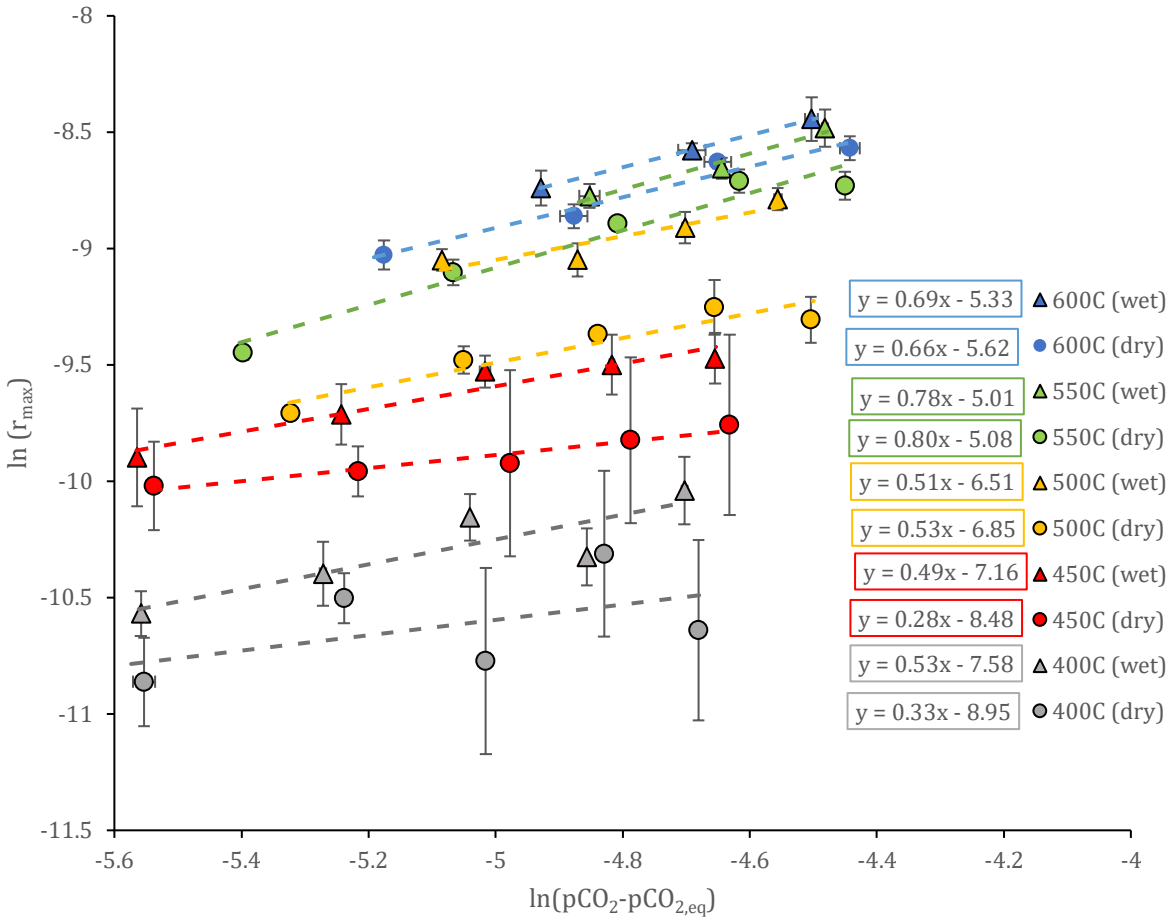

Fig. 5: Plot of $\ln(r_{max})$ against $\ln(p_{CO_2} - p_{CO_2,eq})$ for all temperatures investigated after screening for externally mass transfer limited data points. The linear equations for each trendline are shown next to the corresponding temperature. The error bars depict the 95% confidence interval from three experimental points per $(p_{CO_2} - p_{CO_2,eq})$.

Figure 5 gives a plot of $\ln(r_{max})$ against $\ln(p_{CO_2} - p_{CO_2,eq})$, and, recalling eq. (2), provides the values for n – the order of reaction – directly from the slopes of linear fits. All values of n against the experimental temperatures are also presented in Fig. 6. As discussed earlier, the governing rate expression for carbonation found in literature assumes that the order of reaction with respect to $(p_{CO_2} - p_{CO_2,eq})$ is $n = 1$ for a broad range of $(p_{CO_2} - p_{CO_2,eq})$, commonly defined as <10 kPa. However, the fitted linear equations and values for n in Figs. 5 and 6 do not approach 1 across all temperatures. The range of $(p_{CO_2} - p_{CO_2,eq})$ investigated here spans from 0.3 to 1.2 kPa – a significantly lower range than usually reported. To our knowledge, this is the first study to look into such low driving forces, assessing n and its behaviour against T.

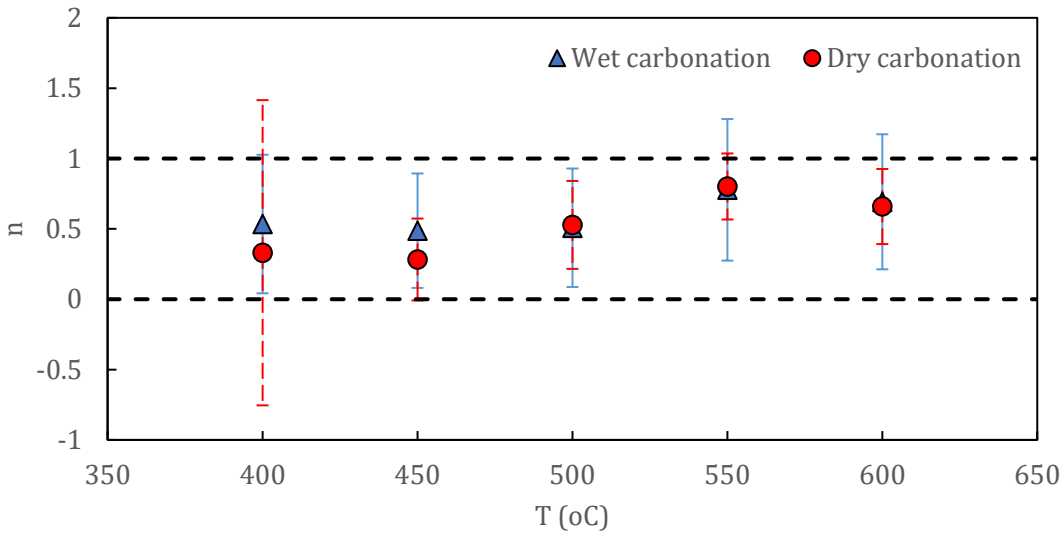

Fig. 6: Plot of n against T for wet and dry carbonation for linear fitted lines in Fig. 5. The black dashed lines illustrate both $n = 1$ and $n = 0$. The error bars indicate the 95% confidence intervals for each temperature data set.

The behaviour of n shifting between 0 and 1 here was unexpected, especially that the assumption of $n = 1$ led to a good linear fit and a small error range for E_A and A from the results in Fig. 4. One potential reason for changes in n could be the non-validity of the assumptions made to derive the rate expression generally used in literature for carbonation but applied to much higher ranges of $(p_{CO_2} - p_{CO_2,eq})$ than used in this work. Most work on carbonation assumes two-step processes – adsorption and chemical reaction. However, an earlier step may also be important. For example, Li *et al.* [20] proposed that $CaCO_3$ creation involves nucleation events, confirmed with atomic force microscopy. In their detailed model of the nuclei occurrence and growth, they considered a rate expression that describes the surface reaction, surface diffusion, as well as diffusion on grain boundaries and through the lattice, and, finally, the Ostwald ripening. Which of those steps could be limiting the rates in our experiments is beyond the scope of this work, but the fact that n changes quickly with T indicates that multiple phenomena might be at play simultaneously. We finally note that the presence of steam has little effect on n, further confirming that the chemical reaction might be limited by another intermediate step.

Taking the experimentally determined values for n, we recalculate k_A as $k_A = \frac{r}{(p_{CO_2} - p_{CO_2,eq})^n}$ and use it again to assess the kinetic parameters. The results are presented in Fig. 7. The achieved values for the activation energy are now significantly higher than in Fig. 4., and closer to 77 kJ/mol obtained by Kyaw *et al.* [21]. Additionally, Ortiz et al. [15] listed that the activation energy for the $CaCO_3$ synthesis step is of the order of 20 kJ/mol, similar to the sorption steps,

while the required activation energy for $CaCO_3$ decomposition is closer to 180 kJ/mol. If the mechanism of carbonation, close to equilibrium, resulted from a mixture of the involved steps without specific limitation from any single one, then the E_A for the apparent k_A would range from 20 to 180 kJ/mol. Thus, overall, we conclude that the carbonation close to the equilibrium limitations, at low temperatures and driving forces represents a mixed multistep process.

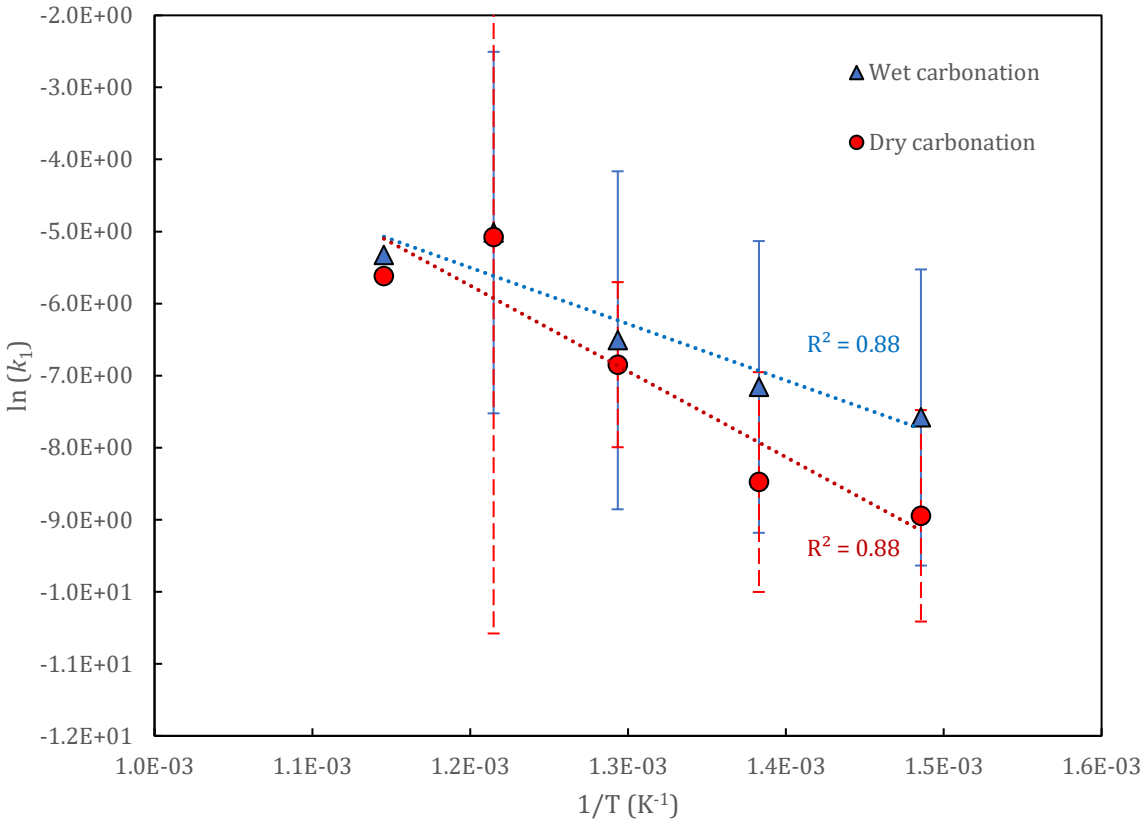

	E_a [kJ mol^{-1}]	A [mol s^{-1} g$_{CaO}^{-1}$ atm^{-1}]
Wet carbonation	65	49
Dry carbonation	99	5,078

Fig. 7: Plot of $\ln(k_A)$ against $1/T$ for wet and dry carbonation, where $\ln(k_A)$ was extracted from the y-axis intercepts of the linear equations in Fig. 5. The error bars indicate the 95% confidence intervals for each temperature.

Recalling from Section 3 that the overall calcium looping reaction $CaO + CO_2 \rightleftharpoons CaCO_3$ was proposed to follow the Langmuir-Hinshelwood mechanism with a surface adsorption-desorption step followed by a chemical reaction step, the rate expression can also be described using the full set of kinetic constants, eq 18.

$$r = \frac{2k_1k_A\left(p_{CO_2} - p_{CO_2,eq}\right)}{k_1 + k_2 + k_A p_{CO_2} + k_D} \tag{18}$$

$$\frac{k_2k_D}{k_1k_A} = p_{CO_2,eq} \tag{19}$$

From here, non-linear fitting of r and p_{CO_2} can be performed to obtain k_1, k_2, k_A and k_D, with the additional constraint from eq. 19. The nonlinear fitting was performed using the *lsqnonlin* function in MATLAB while further constraining the solution values to be positive. Figure 8 shows the result of fitting the data points for r_{max} at various p_{CO_2} and temperatures for dry carbonation.

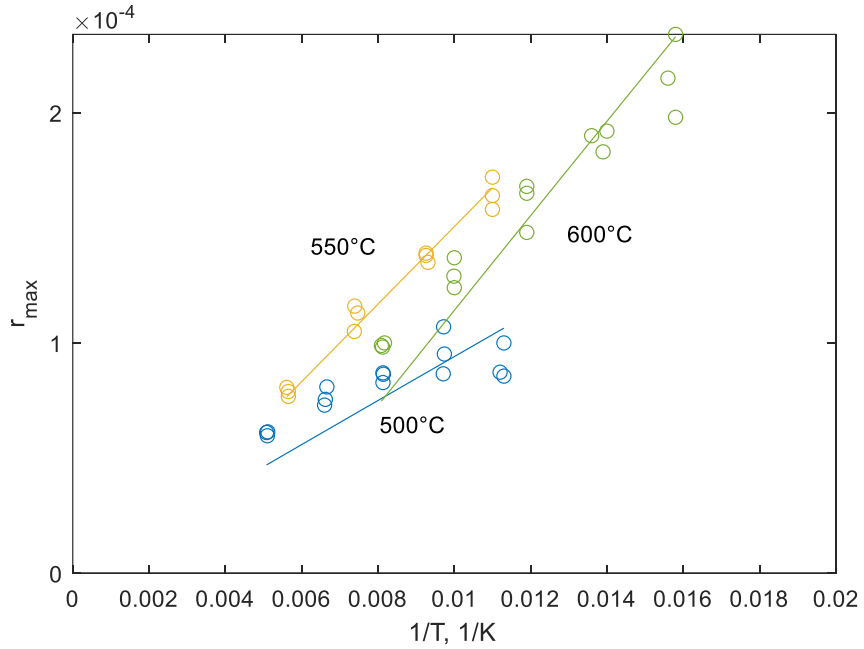

Fig. 8: Plot of r_{max} against $1/T$. The MATLAB *lsqnonlin* built-in function was used to fit k_A, k_D, k_1, k_2 to eqs. (18) and (19) with the experimental r_{max} data.

The parameters obtained as fits to the experimental results gave k_A ~ k_D.Only then, eq. 19 was satisfied. We, thus, conclude that the adsorption-desorption step was at equilibrium, with the kinetics of the chemical reaction limiting the rate, as suggested by Moore for heterogeneous reactions[22]. Assuming the Arrhenius form for k_1 and k_2, we obtained $E_{a,1}$ =4.5 kJ/mol for carbonation, while $E_{a,2}$=31 kJ/mol for the reversed reaction. Both values are low, but their ratio, ~7, is similar to that provided by Ortiz *et al.*, *i.e.* 9 [15]. The results thus suggest the dominating importance of the chemical reaction, possibly affected by additional phenomena, such as the appearance of nuclei of $CaCO_3$[20].

To finish the analysis, we finally estimate the degree in which the reaction was limited by intraparticle mass transfer, using the effectiveness factor, η.

$$\eta = \frac{3}{\phi^2}(\phi \coth(\phi) - 1) \tag{20}$$

where ϕ is the Thiele modulus:

$$\phi = r_p \sqrt{\frac{k_i}{D_{\text{eff}}}} \tag{21}$$

and r_p is the particle radius taken as the geometric mean, and k_i is the pseudo intrinsic first order rate constant in s^{-1}. Next, the effective diffusivity D_{eff} is given as

$$D_{\text{eff}} = \frac{\varepsilon_p}{\tau_p}\left(\frac{1}{D_K} + \frac{1}{D_{AB}}\right)^{-1} \tag{22}$$

where ε_p is the particle porosity taken as 0.5, and τ_p is the tortuosity taken as 2. Then, D_{AB} is the binary diffusion coefficient while the Knudsen diffusivity, D_K is given as

$$D_K = 194 \frac{\varepsilon_p}{S_0 \rho_{env}} \sqrt{\frac{T}{M_{CaO}}} \tag{23}$$

where S_0 is the specific surface area of the particle taken as $9.87 \times 10^6\ \text{m}^2\ \text{m}^{-3}$ and ρ_{env} is the envelope density taken as $1.2 \times 10^6\ \text{g m}^{-3}$ [23], and M_{CaO} is the molar mass of CaO - 56 g mol^{-1}.

Table 1 summarises the estimated values of η for dry carbonation. Given that $\eta \approx 1$ for all investigated conditions, intraparticle mass transfer was deemed a non-factor, and thus, the values of r_{max} observed in this work were instead likely controlled by the surface reaction.

Table 1: Summary of η at the temperatures investigated.

T [°C]	η	ϕ	k_i [s^{-1}]
400	1.00	4.24E-07	1.05E-10
450	1.00	5.60E-07	1.94E-10
500	1.00	2.32E-07	3.53E-11
550	0.99	1.04E-07	7.37E-12
600	0.98	8.26E-08	4.89E-12

5. Conclusions

The carbonation of CaO in a fluidised bed was carried out to investigate the kinetics at near-equilibrium conditions. It was found that when the $(p_{CO_2} - p_{CO_2,eq})$ driving force was between 1×10^{-3} atm to 2.5×10^{-3} atm, the carbonation reaction was limited by external mass

transfer, thus higher CO_2 concentrations were needed to study kinetics. The pseudo-catalytic effect of steam accelerated carbonation in the kinetically controlled regime, albeit with diminishing returns with increasing temperature. At near-equilibrium conditions, the order of reaction, n, varied with temperature and did not reach $n = 1$, *i.e.* the value as commonly assumed in the literature. The obtained kinetic parameters, as well as the variations of n with T indicate the possible influence of phenomena connected to nucleation and the growth of nuclei. Non-linear fitting of kinetic parameters to match the Langmuir-Hinshelwood expression demonstrated that the sorption step was equilibrated. In contrast, the kinetics of carbonation and decarbonation were rate-limiting for low-temperature CO_2 capture, even at low investigated CO_2 concentrations.

Supporting Information Statement

The Supporting Information file contains XRD results, details on data analysis, conversion of CaO particles, fluidisation parameters.

References

(1) Scaltsoyiannes, A.; Antzaras, A.; Koilaridis, G.; Lemonidou, A. Towards a Generalized Carbonation Kinetic Model for CaO-Based Materials Using a Modified Random Pore Model. *Chemical Engineering Journal* **2021**, *407*, 127207. https://doi.org/10.1016/j.cej.2020.127207.

(2) Ruhaimi, A. H.; Aziz, M. A. A.; Jalil, A. A. Magnesium Oxide-Based Adsorbents for Carbon Dioxide Capture: Current Progress and Future Opportunities. *Journal of CO2 Utilization* **2021**, *43*, 101357. https://doi.org/10.1016/j.jcou.2020.101357.

(3) Costagliola, M. A.; Prati, M. V.; Perretta, G. Post Combustion CO2 Capture with Calcium and Lithium Hydroxide. *Sci Rep* **2022**, *12* (1), 10518. https://doi.org/10.1038/s41598-022-14235-5.

(4) Hu, Y.; Liu, W.; Chen, H.; Zhou, Z.; Wang, W.; Sun, J.; Yang, X.; Li, X.; Xu, M. Screening of Inert Solid Supports for CaO-Based Sorbents for High Temperature CO2 Capture. *Fuel* **2016**, *181*, 199–206. https://doi.org/10.1016/j.fuel.2016.04.138.

(5) Hanak, D. P.; Michalski, S.; Manovic, V. From Post-Combustion Carbon Capture to Sorption-Enhanced Hydrogen Production: A State-of-the-Art Review of Carbonate Looping Process Feasibility. *Energy Conversion and Management* **2018**, *177*, 428–452. https://doi.org/10.1016/j.enconman.2018.09.058.

(6) Berstad, D.; Anantharaman, R.; Jordal, K. Post-Combustion CO2 Capture from a Natural Gas Combined Cycle by CaO/CaCO3 Looping. *International Journal of Greenhouse Gas Control* **2012**, *11*, 25–33. https://doi.org/10.1016/j.ijggc.2012.07.021.

(7) Ortiz, C.; Valverde, J. M.; Chacartegui, R.; Benítez-Guerrero, M.; Perejón, A.; Romeo, L. M. The Oxy-CaL Process: A Novel CO2 Capture System by Integrating Partial Oxy-Combustion with the Calcium-Looping Process. *Applied Energy* **2017**, *196*, 1–17. https://doi.org/10.1016/j.apenergy.2017.03.120.

(8) Romano, M. C.; Anantharaman, R.; Arasto, A.; Ozcan, D. C.; Ahn, H.; Dijkstra, J. W.; Carbo, M.; Boavida, D. Application of Advanced Technologies for CO2 Capture From Industrial Sources. *Energy Procedia* **2013**, *37*, 7176–7185. https://doi.org/10.1016/j.egypro.2013.06.655.

(9) Dunstan, M. T.; Donat, F.; Bork, A. H.; Grey, C. P.; Müller, C. R. CO2 Capture at Medium to High Temperature Using Solid Oxide-Based Sorbents: Fundamental Aspects, Mechanistic Insights, and Recent Advances. *Chem. Rev.* **2021**, *121* (20), 12681–12745. https://doi.org/10.1021/acs.chemrev.1c00100.

(10) Grasa, G. S.; Abanades, J. C. CO2 Capture Capacity of CaO in Long Series of Carbonation/Calcination Cycles. *Ind. Eng. Chem. Res.* **2006**, *45* (26), 8846–8851. https://doi.org/10.1021/ie0606946.

(11) Bale, C. W.; Bélisle, E.; Chartrand, P.; Decterov, S. A.; Eriksson, G.; Gheribi, A. E.; Hack, K.; Jung, I.-H.; Kang, Y.-B.; Melançon, J.; Pelton, A. D.; Petersen, S.; Robelin, C.; Sangster, J.; Spencer, P.; Van Ende, M.-A. FactSage Thermochemical Software and Databases, 2010–2016. *Calphad* **2016**, *54*, 35–53. https://doi.org/10.1016/j.calphad.2016.05.002.

(12) Sun, P.; Grace, J. R.; Lim, C. J.; Anthony, E. J. Determination of Intrinsic Rate Constants of the CaO–CO2 Reaction. *Chemical Engineering Science* **2008**, *63* (1), 47–56. https://doi.org/10.1016/j.ces.2007.08.055.

(13) Yu, F.-C.; Fan, L.-S. Kinetic Study of High-Pressure Carbonation Reaction of Calcium-Based Sorbents in the Calcium Looping Process (CLP). *Ind. Eng. Chem. Res.* **2011**, *50* (20), 11528–11536. https://doi.org/10.1021/ie200914e.

(14) García-Labiano, F.; Abad, A.; de Diego, L. F.; Gayán, P.; Adánez, J. Calcination of Calcium-Based Sorbents at Pressure in a Broad Range of CO2 Concentrations. *Chemical Engineering Science* **2002**, *57* (13), 2381–2393. https://doi.org/10.1016/S0009-2509(02)00137-9.

(15) Ortiz, C.; Valverde, J. M.; Chacartegui, R.; Perez-Maqueda, L. A. Carbonation of Limestone Derived CaO for Thermochemical Energy Storage: From Kinetics to Process Integration in Concentrating Solar Plants. *ACS Sustainable Chem. Eng.* **2018**, *6* (5), 6404–6417. https://doi.org/10.1021/acssuschemeng.8b00199.

(16) Davidson, J. F.; Harrison, D. *Fluidised Particles*; Cambridge University Press, 1963.

(17) Kwong, K. Y.; Harrison, A. R. P.; Gebers, J. C.; Dennis, J. S.; Marek, E. J. Chemical Looping Combustion of a Biomass Char in Fe2O3-, CuO-, and SrFeO3−δ-Based Oxygen Carriers. *Energy Fuels* **2022**, *36* (17), 9437–9449. https://doi.org/10.1021/acs.energyfuels.2c01269.

(18) Hernández-Jiménez, F.; Gómez-García, A.; Santana, D.; Acosta-Iborra, A. Gas Interchange between Bubble and Emulsion Phases in a 2D Fluidized Bed as Revealed by Two-Fluid Model Simulations. *Chemical Engineering Journal* **2013**, *215–216*, 479–490. https://doi.org/10.1016/j.cej.2012.10.056.

(19) Manovic, V.; Anthony, E. J. Carbonation of CaO-Based Sorbents Enhanced by Steam Addition. *Ind. Eng. Chem. Res.* **2010**, *49* (19), 9105–9110. https://doi.org/10.1021/ie101352s.

(20) Li, Z.; Sun, H.; Cai, N. Rate Equation Theory for the Carbonation Reaction of CaO with CO2. *Energy Fuels* **2012**, *26* (7), 4607–4616. https://doi.org/10.1021/ef300607z.

(21) Kyaw, K.; Kubota, M.; Watanabe, F.; Matsuda, H.; Hasatani, M. Study of Carbonation of CaO for High Temperature Thermal Energy Storage. *Journal of Chemical Engineering of Japan* **1998**, *31* (2), 281–284. https://doi.org/10.1252/jcej.31.281.

(22) Moore, W. J. *Physical Chemistry (5th Edition)*; Prentice-Hall, 1972.

(23) Manovic, V.; Charland, J.-P.; Blamey, J.; Fennell, P. S.; Lu, D. Y.; Anthony, E. J. Influence of Calcination Conditions on Carrying Capacity of CaO-Based Sorbent in CO2 Looping Cycles. *Fuel* **2009**, *88* (10), 1893–1900. https://doi.org/10.1016/j.fuel.2009.04.012.